POLITECNICO DI TORINO
Repository ISTITUZIONALE

Characterization of Co-Cr-Mo alloys after a thermal treatment for high wear resistance

Original
Characterization of Co-Cr-Mo alloys after a thermal treatment for high wear resistance / Balagna, Cristina; Spriano, Silvia Maria; Faga, M. G.. - In: MATERIALS SCIENCE AND ENGINEERING. C, BIOMIMETIC MATERIALS, SENSORS AND SYSTEMS. - ISSN 0928-4931. - 32:7(2012), pp. 1868-1877. [10.1016/j.msec.2012.05.003]

Availability:
This version is available at: 11583/2497188 since:

Publisher:

Published
DOI:10.1016/j.msec.2012.05.003

Terms of use:
openAccess

This article is made available under terms and conditions as specified in the corresponding bibliographic description in the repository

Publisher copyright

(Article begins on next page)

05 May 2023

Characterization of Co-Cr-Mo alloys after a thermal treatment for high wear resistance

C.Balagna[a, *],S.Spriano[a] , M.G. Faga[b]

This is the author post-print version of an article published on *Materials Science and Engineering: C*, Vol. *32*, n. *7*, pp. *1868-1877*, *2012* (ISSN *0928-4931*).
The final publication is available at
http://dx.doi.org/10.1016/j.msec.2012.05.003
This version does not contain journal formatting and may contain minor changes with respect to the published edition.
The present version is accessible on PORTO, the Open Access Repository of the Politecnico of Torino, in compliance with the publisher's copyright policy.
Copyright owner: *Elsevier*.

[a]*Institute of Materials Physics and Engineering, Department of Applied Science and Technology*

Politecnico di Torino, Corso Duca degli Abruzzi 24,10129 Torino, Italy

[b]*Istituto di Scienza e Tecnologia dei Materiali Ceramici,*

Consiglio Nazionale delle Ricerche, Strada delle Cacce 73, 10135 Torino, Italy

[*]*Corresponding author: Tel.:* +39 011 5644668; *Fax* : +39 011 5644699;

E-mail address: cristina.balagna@polito.it

Abstract

The cobalt-chromium-molybdenum alloys are characterized by a high resistance to wear and corrosion, as well as good mechanical properties, allowing their use in the substitution of hip and knee joints.

Five alloys were used as substrates for a coating deposition by a thermal treatment in molten salts, as reported elsewhere, in order to form a tantalum rich coating on the sample surface, able to improve the biocompatibility and wear resistance of the materials. However, the temperature (970°C), reached during this process, is considered critical for the phase transformation of the Co-based alloys.

The aim of this work is the evaluation of the temperature effects on the structure, microstructure, mechanical and tribological properties of the considered substrates, after the removal of the coating by polishing. The substrates are characterized through X-ray diffraction (XRD), scanning electron microscopy with energy dispersion spectrometry (SEM-EDS) and profilometry. The mechanical behaviour is evaluated by the macro- and micro-hardness and bending tests, whereas the tribological properties are analyzed through a ball on disc test. A comparison between the as-received alloys and thermal treated substrates is reported. The biocompatibility feature is not reported in this work.

The substrate crystalline structure changed during the heat treatment, inducing the formation of the hexagonal cobalt phase and the decrement of the cubic one. This crystallographic modification does not seem to influence the tribological behaviour of the substrates. On the contrary, it affects the strength and ductility of the substrates.

Keyword: CoCrMo alloys, Heat treatment, Microstructure, Wear resistance, Arthroprosthesis

1. Introduction

The cobalt-chromium-molybdenum (CoCrMo) alloys can be used in the artificial replacements of human hip and knee joints because of their good wear and corrosion resistance, as well as their mechanical strength [1, 2]. The CoCrMo component of a prosthesis usually articulates on the same alloy, on ultra high molecular weight polyethylene (UHMWPE) or on alumina, forming a metal on metal (MoM), metal on polyethylene (MoP) or metal on ceramic (MoC) joint, respectively [3,4]. The knee joints, instead, are typically substituted with a MoP system [3].

The wear and corrosion of the bearing surfaces remain the principal causes of the early failure of the implants, despite of the wide use of these materials and the improvements in the technique and design of the implants, as well as in the surgical methods [4, 5]. The UHMWPE element is the most critical in the wear feature because of the formation of debris, contributing to osteolysis [5-7]. Alternatively, the MoM and MoC couplings are considered suitable for younger and more active patients because the wear of articulating surfaces is significantly reduced [8, 9]. However, the CoCrMo alloys can be affected by the synergic action of both corrosive human body fluids and friction [5, 10, 11]. In fact, metallic ions and particles are formed in a smaller size, but in a higher number than the polyethylene debris [12-15]. Wear debris and ions could remain in the implant site or be disseminated into the other organs and lymph nodes [16, 17], increasing the risk of hypersensitivity or inducing a cascade of inflammatory events [7, 12, 18-21].

The tribological and mechanical properties of the Co-based alloys strongly depend on their microstructure [22-24]. In the CoCrMo alloys, the face-centered cubic (FCC) and the hexagonal closed packed (HCP) crystalline structures co-exist. Typically, the FCC phase is predominant at room temperature, but the FCC→HCP transformation could be isothermally or strain- induced [23, 25, 26]. The other main feature of the Co-based alloys is the presence of carbon forming carbides whose distribution and size is influenced by the manufacturing process [27, 28]. The main factors that affect the wear resistance of CoCrMo alloys are the carbon amount, the homogeneity of the

carbides distribution and the presence of the HCP crystal structure [10, 13, 29]. However, some contrasting studies are reported in literature on this last topic. It was verified that a tribological system with an almost fully complete HCP structure on both the sliding components exhibits a lower wear loss comparing to the FCC structure [24]. On the contrary, *Varano and co-workers* [22] stated that the alloys with a higher amount of the FCC phase, stabilized by the carbon content, which inhibits the martensitic transformation, exhibit lower wear, because the HCP crystalline structure is more brittle and detrimental to wear. The carbides influence the wear by means the hardness and the good coherency with the surrounding matrix, acting as a protective barrier against the matrix delamination [22]. However, the high hardness of the carbides could cause abrasive wear damage, when they are pulled-out and fractured from the matrix, decreasing the resistance to the surface fatigue [23].

This work is focused on the influence evaluation of a thermal treatment in molten salts on the mechanical and wear properties of several implant CoCrMo alloys, different in carbon content and manufacturing processes. The thermal treatment in molten salts was performed at a temperature (970°C) recognized as critical for the CoCrMo alloys, promoting the FCC→HCP martensitic transformation [26, 41, 42]. This temperature was set because it allows the formation of a peculiar coating on the alloy surface, as reported in the previous works of the authors [30-33]. The coating was composed of a multilayer structure of tantalum carbides, and it is able to improve the biocompatibility as well as the wear and corrosion resistance of the alloys. The well-known biocompatible behaviour [34-37], excellent mechanical and tribological properties, as well as corrosion resistance [38-40] of tantalum (Ta) and its compounds are shown on the coating. In addition, it was observed by the authors that the mechanism of coating formation was the diffusion of the tantalum from the salts to the alloy surface and the reaction of the tantalum with the carbon contained in the Co-based substrate. It must be underlined that the substrate below the coating can be affected by the employed temperature and the chemical surface reaction occurred during the coating formation.

The aim of this work is to investigate if the different CoCrMo substrates are affected by any micro-structural or mechanical changes. The carbides, present in the substrate, could be subjected to a modification in the dimension, quantity and distribution, during the thermal treatment. The treated alloys were evaluated after the complete removal of the coating and a comparison with the as-received materials is reported in the paper. The metal ions release relative to the as-received alloys and the coated samples was controlled in a previous work [30].

2. Materials and Methods

2.1 The substrates

Five CoCrMo alloys, different in the composition, carbon content and manufacturing process, were considered. Three of them were characterized by a high carbon content (HC) and they were produced by wrought processing (W), powder metallurgy (PM) or casting (C). The other two contained a low carbon amount (LC) and they were manufactured by means of a wrought processing or casting. All the alloys were supplied by Smith & Nephew Inc. in a disk-shape, with a diameter of 30 mm and thickness of 3 mm, with a mirror polished surface. The carbon content was evaluated by optical spectrometry (Spectro - Spectrolab 5) while the other alloying elements were quantified through energy dispersion spectrometry (SEM-FEI, Quanta Inspect 200, EDS - EDAX PV 9900), at a voltage of 15kV.

The as-received CoCrMo alloys were thermal treated in a mixture of Ta-rich salts using a patented method [33], well described in previous works [30-32]. The thermal process was carried out at 970°C for 45 minutes, in a tubular furnace, under a controlled Ar atmosphere. The sample was completely dipped into the salts mixture, composed predominantly of K_2TaF_7 and 2wt.% of Ta, during the whole treatment. A Ta-based coating was formed on the sample surface and then it was completely removed by a careful polishing procedure with SiC papers from 600 to 4000 grit, until obtaining a mirror-polished surface, in order to analyse the substrates. The treated substrates, so obtained, will be named by adding the employed isothermal temperature and the suffix “sub” to the

name of alloy (such as HC-C970sub). The weight loss and thickness of the removed material layer, with polishing, were measured about 2-3 g and 0.45-0.49 mm, respectively. The LC-C970sub sample was an exception, because of the lower thickness of its coating (the removed material was 1.2 g and 0.08 mm).

2.2 Sample characterization

The roughness of all the samples was measured by means of a contact profilometer (Tencor P-11), acquiring three typical parameters, the arithmetical mean roughness (Ra), root mean square value (Rq) and ten-point mean roughness Rz. Three measurements were performed for each sample in order to obtain statistical data.

The X-ray diffraction measurements (XRD, X'Pert Philips diffractometer) were performed on the as-received alloys and treated substrates, with the Bragg–Brentano camera geometry, the Cu Kα incident radiation, at 40kV of voltage and 30mA of current, in a 2Theta range among 30 and 90 degrees. The X'Pert High Score software and PCPDF data bank were used to accomplish the pattern analysis of crystalline phases. The relative amounts of FCC and HCP phases were estimated by measuring the integrated intensities of the principal peaks of this two phases, I_{200}^{fcc} and $I_{10\bar{1}1}^{hcp}$. The volume fraction of the HCP phase was calculated using the expression developed by Sage and Gillaud [43] and typically employed by Saldivar also [26]:

(1) $$f^{hcp} = \frac{I_{10\bar{1}1}^{hcp}}{I_{10\bar{1}1}^{hcp} + 1.5 I_{200}^{fcc}}$$

Another method, used in order to calculate the percentage volume fraction of a phase ($f^{phaseA}(\%)$), was the following ratio:

(2) $$f^{phaseA}(\%) = \frac{\sum I_{peaksA}}{\sum I_{peaksTot}} \times 100$$

where A is the considered phase, $\sum I_{peaksA}$ is the sum of the intensities of all the peaks belonged to the considered phase, $\sum I_{peaksTot}$ is the sum of the intensities of all the peaks in the diffractogram.

A further investigation, for determining the phase amount and the crystal size, was performed by using a program of Material Analysis Using Diffraction, called MAUD and developed at the University of Trento. It is a general diffraction/reflectivity analysis program mainly based on the Rietveld method.

The microstructure of the as-received alloys and treated substrates was analyzed. First, the metallic carbides were observed by means of a scanning electron microscopy and energy dispersion spectrometry (SEM-EDS, Philips 525M) at the voltage of 15 kV and by an optical microscope. Afterwards, an etching procedure was performed, dipping all the samples for 5-10 seconds in an acid solution of HCl and H_2O_2 (20:1) [44]. The optical microscope was used for the observation of the grains.

The disk hardness was estimated by means of micro- and macro-indentation using a Vickers indenter in both cases (Leitz Microvickers Penetrator and Dia Testor 2 RC- Wolpert). The applied loads were 100g and 500 g for micro-indentation test and 40 kg for macro-indentation. Five measurements for each samples were performed in order to obtain statistical data. The mechanical resistance of the as-received alloys and the treated substrates was determined by means of a 3-point bending test (MTS QTest/10). The samples were cut from the disks, obtaining rectangular cross-sectioned bars with dimensions in accordance to ISO 3327-1982 standard [45]. The maximum applied load was equal to 10 kN, reached with a load rate of 1 mm/min. The transverse rupture strength σ (MPa), the maximum bending deformation ε and the flexural elastic modulus E (GPa) were calculated trough :

$$\sigma = \frac{3 \times P \times L}{2 \times b \times d^2} \quad (3)$$

(4) $$\varepsilon = \frac{6 \times D \times d}{L^2}$$

and

(5) $$E = \frac{m \times L^3}{4 \times b \times d^2}$$

where P (N) is the failure load, L (mm) is the distance between the supports, representing the useful sample length, and it varied between 16.5 and 18.5 mm, b and d (mm) are the width and height of the rectangular cross-sectioned samples, respectively, D (mm) is the deflection at the failure load of the center of the tested sample and m (N/mm) is the gradient of the initial straight-line part of the load-deflection curve. The dimensions of the sample cross-sections are reported in Table 1. A single sample was tested for each kind of alloy.

Finally, the ball on disc test was performed in order to investigate the wear behaviour of the as received alloys and treated substrates, using a CSEM high temperature tribometer. An alumina ball covered 25000 laps under an applied load of 7 N and with a linear speed of 10 cm/s. The radius of the circumference was fixed, during the whole test, at 7 mm. The test was carried out at the human body temperature (37°C) in a wet environment, using dilute bovine serum as lubricant. The lubricant was prepared as a solution of 25% vol. of calf bovine serum and 75%vol. of distilled water with the addition of sodium azide (Na_3N) as antibacterial agent in the ratio of $1gl^{-1}$. The sodium azide allows the stock for longer time of the bovine serum solution, avoiding the bacterial contamination. The wear track profiles were evaluated through a profilometer and the morphology of the wear tracks were observed by SEM.

3. Results and Discussions

3.1 The as-received alloys and the preparation of the treated substrates

The as-received CoCrMo alloys differ in composition, carbon content and in the manufacturing technology (powder metallurgy, plastic deformation or casting). Data relative to the acronymous,

manufacturing technique and composition of the as-received materials are summarized in Table 2. The carbon present in the HC alloys exceeds 0.1 wt.%, while the content in the LC samples is 0.07 wt.% in the casting alloy and less than 0.01 wt.% in the wrought alloy. The alloying elements are similar in composition in all the materials, except for nickel that was only detected in a very low quantity in the HC-W, HC-C and LC-W alloys. The carbon amount of the different alloys mainly influences the formation and precipitation of carbides in the matrix [27], whereas the manufacturing procedure typically affects the distribution and shape of the carbides [22].

The alloys were used as substrates in a thermal treatment in molten salts, performed at 970°C for 45 min, in order to induce the formation of a tantalum-rich coating on the alloy surface, able to improve the mechanical, wear and biocompatible behavior. The authors observed, in previous works [31, 32], that the process under these precise conditions formed a peculiar coating, composed of a multilayer structure of tantalum carbides. However, two relevant aspects arose concerning the CoCrMo substrates. First of all, the treatment was performed at a temperature known as critical for the martensitic transformation of the cobalt crystalline structure. Secondly, the mechanism of the coating formation is diffusion-type and the tantalum, belonged to the salts, reacts with the carbon of the CoCrMo substrate, to form the tantalum carbides phase, present in the coating. These features could induce some changes also into the structure, microstructure and correlative properties of the substrates.

The coated samples were polished in order to completely remove the coating and well-polished surfaces were obtained. They have a roughness comparable to the as-received samples, according to the standard for the prostheses [46] (Table 3).

3.2 The crystalline structure and microstructure

Fig. 1 shows the SEM images relative to the as-received alloys (on the left) and the substrates (on the right), reporting also the EDS analysis on several areas. Both the HC-W (Fig.1a) and HC-PM (Fig.1c) alloys show homogeneously distributed carbides inside the matrix. The samples,

obtained by powder metallurgy, contain, as usually, finer carbides than the wrought ones, maintaining their dimension in the range of few micrometers. In the case of the cast alloys (Fig.1 e and f, respectively), the carbides shape, dimension and distribution completely differ from the other two alloy types. In fact, the carbides are less in number and they appear as agglomerates and blocks into the matrix. Two kinds of carbides are noticed. The EDS analysis, reported in Fig. 1, suggests that the light grey-white carbides contain a large amount of Mo (l), whereas the black-dark grey carbides mainly contain Cr (i). In the cast alloys, the Mo carbides are larger (higher than 5 μm) and with an irregular shape. On the contrary, the Cr carbides are smaller, presenting a circular and regular shape. The carbides precipitated in the LC-C alloy are similar in distribution to the HC-C sample, but fewer and larger. No photos about the LC-W alloy are reported because no carbides were detected in this sample by SEM-EDS. The thermal treatment, performed in molten salts at 970°C, did not change the dimension, shape and distribution of the carbides, as it can be observed by the comparison among the alloys before and after the process (Fig.3 b, d, f, h).

These results are congruent with those reported in literature [25, 28]. In fact, it is well known that the carbide dissolution may happen only for a solution treatment performed at a temperature above 1150°C. It can be concluded that the tantalum carbides which formed the coating did not affect the Mo and Cr carbides of the substrate.

Fig. 2 and 3 reported the XRD diffractograms with a comparison before and after the thermal treatment for each alloy. It can be seen that the temperature reached in the thermal process, induced a martensitic transfomation of FCC phase into HCP phase, confirming the studies conducted by *Saldivar – Garcia and co workers*. It is reported that FCC phase easily transforms into HCP phase during a thermal treatment of ageing at temperatures between 800-950°C [24-26, 41, 42]. The CoCrMo alloys are typically characterized by the presence of two cobalt crystalline structures, the cubic (FCC Co, PCPDF reference code 01-089-4307) and hexagonal (HCP Co, PCPDF reference code 01-089-4308). As it could be observed, the three peaks of the FCC Co are noticed for all the as-received alloys even if the LC-C alloys (Fig.3 b) presents a weak peak of FCC around 44°. In

addition, the relative intensity of the FCC peaks, in the cast alloys (Fig. 2c and 3b), is different with respect to the other substrates, due to a preferential orientation caused by the manufacturing process. An increment in the HCP amount is verified after the thermal treatment in all the diffractograms, confirming the data from literature. In fact, the HC-W970sub (Fig. 2a) and the LC-W970sub (Fig.3a) samples show not only higher intensity of the two peaks at 41° and 47°, already detected in the untreated alloys, but also the appearance of two other peaks around 62° and 84° which were absent before the treatment. The thermal treatment induced a further re-distribution between FCC peaks in the cast materials (HC-C970sub, LC-C970sub) where a preferential orientation is observed. Table 4 summarizes the volume fraction of the amount of the HCP and FCC crystalline structures inside the alloys, estimated through (1), (2) and MAUD program. The data obtained for the as-received wrought and powder metallurgy alloys are very similar comparing all the methods of calculations. However, the values concerning the cast materials and all the treated substrates are different and some contrasting results are obtained, comparing the different analyses. Estimations from both the Sage and Guillaud's formula and Rietveld-MAUD method has to be considered not significant and precise for these samples. The preferential orientation of both the FCC and HCP phases in the cast materials made invalid the measurements performed by these two methods, which consider only the HCP peak with 100% of relative intensity in the PCPDF pattern and the FCC peak with 40% of relative intensity in the PCPDF pattern. On the other hand, the formula (2) considers all the peaks in the diffractogram so it is less sensitive to preferential orientations. In conclusion, the high carbon alloys approached to a similar percentage volume fraction of the HCP phase, after the thermal treatment, while a larger disparity was noticed in the low carbon samples, in particular in the LC-C alloy where the HCP phase was significantly more increased.

Fig. 4 reports some optical images of the microstructures relative to the as-received alloys and treated substrates, after etching. The arrows and the circles indicated some grain boundaries and carbides, respectively. The manufacturing technique deeply influences the alloy microstructure. In

fact, the HC-W alloy (Fig.4a) consists of a fine structure with an average grain size around 10 μm and with a relevant presence of carbides. The grains in the HC-PM sample (Fig.4c) are larger than in the wrought alloy, reaching dimensions between 10 and 20 μm, but with a finer carbides distribution at the grain boundaries. Finally, the cast alloys (Fig.4e and g) show a similar coarse microstructure with very large grains (above 100 μm for the HC-C alloy and above 200 μm for the LC-C alloy) and a significant amount of the dark HCP phase, nucleated at the grain boundaries. The thermal treatment, performed at 970°C for 45 min, relevantly affected the sample microstructure and grain dimensions and the progressive formation of the HCP structure occurred in all the analyzed samples. The HCP phase is morphologically identified as a dark phase inside the light grey FCC matrix. The thermal treatment seems to refine the grain size in the HC-Wsub970 (Fig.4b) and HC-PMsub970 (Fig.4d), in contrast with the cast alloys where the grains result further increased. In particular, the grains in the LC-C970sub (Fig.4h) result very large and only part of a grain boundary (indicated by arrows) but not the complete grain can be observed at this magnification in the reported figure. In addition, some white carbides are noticed (dark circle). Considering the cast alloys, the thermal treatment was able to promote the development of the elongated HCP plates along the FCC dendrites or a high density of short plates close to the carbides [24, 41]. The formation of the HCP phase as very fine interdendritic striations starts to nucleate close to the precipitated carbides in the HC-C970 alloy (Fig.5a) or only at the grain boundaries in the LC-C970 alloy (Fig.5b) [41].

3.3 Mechanical properties

Table 5 reports the values of the micro- and macro-hardness obtained from the tests with a Vickers indentator under different loads. The thermal treatment, generally, decreased the hardness of the substrates, especially those containing a high carbon content. On the contrary, the LC-C970sub sample shows a slight increment.

The flexural resistance and ductility was tested through a bending test. A decrement of the ductility was detected after the thermal treatment. The displacement-load curves and data are reported in Fig. 6 and Table 6. The maximum deflection (D) and the failure load (P) were directly obtained from the curves, whereas the transverse rupture strength (σ), the maximum bending deformation (ε) and the flexural elastic modulus (E) were calculated by using the formulas (3), (4) and (5). The Young's modulus increased after the treatment, showing a rigid behavior of the substrates. The treated substrates support higher rupture strengths, but lower deformations. An image of the surface fracture of the HC-W970sub sample is reported as an example in Figure 7. It shows the presence of many fragile fractured Cr carbides in a moderate ductile matrix, where some dimples are noticed. A shear lip is also observed on the fracture surface.

The formation of a large amount of hard HCP phase induced an increment in brittleness and it significantly lowered the strength of the substrates. Considering the XRD analysis (Fig.2 and 3) and the percentage quantities of the phases reported in the Table 4, the starting amount of HCP phase in HC-W and HC-PM samples was low and this was in agreement with the highest values of the registered maximum stress (about 7200N and 7800 N, respectively). In addition, the increment of HCP resulted more relevant for the LC-C970sub sample, followed by the HC-W970sub, HC-PM970sub and HC-C970sub samples, explaining the difference of strength and ductility between the as-received alloys and treated substrates.

3.4 Tribological behavior

The profiles of the wear track sections of the as-received alloys and treated substrates are reported in Fig. 8. The HC-C sample demonstrated the best wear behavior among the untreated alloys, with a track volume (0.02 mm^3) and wear rate (3 x 10^{-6} mm^3/Nm) one order of magnitude lower than the HC-W (0.2 mm^3 and $2x10^{-5}$ mm^3/Nm) and the HC-PM (0.1 mm^3 and $1x10^{-5}$ mm^3/Nm). Also the track section is only 3 μm deep (Fig.8 c), in contrast with 8 or 9 μm values relative to the HC-W (Fig.8a) and HC-PM (Fig.8b) alloys. This could be ascribable to the peculiar

microstructure and carbide distribution of the cast alloys. The comparison with the literature [22, 23] is difficult, because a different counterpart, as well as applied load and sliding distance were used. The track profile relative to the treated substrates (Fig.8) results almost overlapped to the as-received alloys, except for the LC-C sample. In this case, the LC-C970sub sample (Fig.8d) exhibits a narrower, but higher track section than the as-received sample. Even if the amount of the HCP phase inside the bulk, induced by the thermal treatment, may enhance the tribological properties of the material, no relevant differences were noticed in term of wear resistance in the alloys before and after the thermal treatment. This could be explained with the fact that the HCP phase was formed also in the untreated material by a strain-induced martensitic transformation during the wear test, caused by the applied load [23]. Hence, the tribological results, obtained for the as-received alloys, referred to a material containing on the surface an HCP amount higher than that evaluated through XRD analysis. The two peaks visible at the edge of the tracks relative to the HC-W, HC-PM and LC-C as received and treated alloys were correlated to displaced and piled up material, removed with the ball passage.

The predominant wear mechanism consists in abrasion with the contribution of third-body damage both before and after the thermal treatment. In fact, the typical features of the abrasion wear, as scratches and grooves, are noticed inside the tracks of the high carbon cast alloys as reported in Fig. 9. The sample surface was principally abraded by the passage of the hard alumina ball which created deep scratches along its direction. In addition, it is well known that the mean size, volume fraction and distribution of the carbides contribute to the final wear resistance. Hence the Cr and Mo carbides, embedded into the alloys matrix, affected also the wear behavior of the as received alloys, especially in the case of the high carbon content samples. Hard carbides could crack, fracture and pull-out during wear in contact with another hard phase causing third body damage. Moreover their high hardness is considered a relevant cause of abrasive damage. In any case, if they have good coherency with the surrounding matrix might act as a barrier to the matrix delamination [22]. Hence the improved wear performance of the HC-C alloy could be also

attributed to the presence of agglomerates and less numerous carbides inside the matrix, in comparison with the larger number of them in the HC-W and HC-PM alloys. The Mo carbides (light circle) are well visible in the wear track of the HC-C alloy (Fig.9) and a hole left by a Cr carbide (dark circle), pulled out from the surface, is observed in the microphotograph at higher magnification, on the right in Fig. 9. Cr and Co ions were found into the serum bovine, analyzed in the previous authors' work [30], after the wear tests comparing the solution used for the test between alumina ball and as-received alloys and the test between alumina ball and Ta-coated samples. In the first case, the metal ions amount was significantly higher than in the second case, demonstrating that the tantalum coating deposited through thermal treatment in molten salt was able to reduce the release of potential toxic metal ions. The thermal treatment should not influence the ions release of the CoCrMo substrates, however other analysis will be performed in order to control this aspect and the possible cytotoxic behavior.

4. Conclusions

In conclusion, the properties of the CoCrMo alloys are affected by the tested thermal treatment in molten salts. The aim of the treatment was the formation of a Ta-rich coating, but its effects on the substrates cannot be omitted.

Firstly, the temperature induced an increment in the amount of the HCP phase inside the substrates, then it changed the grain size of the matrix. It did not influence the dimension, distribution and size of the carbides. In addition, all the treated substrates were characterized by a preferential orientations of the FCC phase. As a consequence, a decrement in the hardness, especially for the HC alloys, and in the bending ductility was noticed after the thermal treatment. An increment in the flexural strength was also observed after the thermal treatment. In contrast, no significant differences in the tribological properties were obtained, comparing the as-received alloys and treated substrates. The HCP phase was probably induced also onto the as-received alloys during

the wear tests, through a strain-induced mechanism of phase transformation, due to the applied load. The tribological behavior is more strictly related to the carbide presence than to the crystallographic structure. Further work will be needed in order to verify the eventual cytotoxicity of the metal ions released during wear test.

Acknowledgements

Authors would like to thank Smith & Nephew Orthopaedics AG that contributed to the realization of this study with the supply of CoCrMo alloys analysed in this work.

References

[1] A. Marti, Int. J. Care Injured 31 (2000) S-D18-21.

[2] M. Niinomi, Metall. Mater. Trans. A 33 (2002) 477-486.

[3] S.M. Kurtz, Elsevier Academic Press, San Diego (2004).

[4] A. Buford, T. Goswami, Mater. Des. 25 (2004) 385-393 .

[5] T.P. Schmalzried, J.J. Callaghan, J. Bone Jt. Surg. 81A (1999) 114-136.

[6] E. Ingham, J. Fisher, Biomaterials 26 (2005) 1271-1286.

[7] E.Ingham, J. Fisher, Proc. Instn. Mech. Engrs. H 214 (2000) 21-37.

[8] V.D. Shetty, R.N. Villar, Proc. Instn. Mech. Engrs. H 220 (2006) 371-377.

[9] P.J. Firkins, J.L. Tipper, E. Ingham, M.H. Stone, R. Farrar, J. Fisher, J. Biomec. 34 (2001) 1291–1298.

[10] Y. Yan, A. Neville, D. Dowson, Wear 263 (2007) 1105-1111.

[11] D.Sun, J.A. Wharton, R.J.K. Wood, L.Ma, W.M. Rainforth, Tribol. Int. 42 (2009) 99-110.

[12] A.G. Cobb, T.P. Schmalzreid, Proc. Instn. Mech. Engrs. H 220 (2006) 385- 398.

[13] W. T. Long, M.D., Iowa Orthop. J. 25 (2005) 10–16.

[14] J.L. Tipper, P.J. Firkins, A.A. Besong, P.S.M. Barbour, J. Nevelos, M.H. Stone, E. Ingham, J. Fisher, Wear 250 (2001) 120-128.

[15] L. Savarino, D. Granchi, G. Ciapetti, E. Cenni, A. NardiPantoli, R. Rotini, C.A. Veronesi, N. Baldini, A. Giunti, J. Biomed. Mater. Res.: Appl. Biomater. 63 (2002) 467-474.

[16] R.M. Urban, J.J. Jacobs, M.J. Tomlinson, J. Gavrilovic, J.Black, M. Peoc'h, J. Bone Jt. Surg. 82A (2000) 457-477.

[17] C.P. Case, V.G. Langkamer, C. James, M.R. Palmer, A.J. Kemp, P.F. Heap, L. Solomon, J.Bone Jt. Surg. 76-B (1994) 701-712.

[18] C. Brown, J. Fisher, E. Ingham, Proc. Instn. Mech. Engrs. H 220 (2006) 355-369.

[19] O.L. Huk, I. Catelas, F. Mwale, J. Antoniou, D. J. Zukor, A. Petit, J. Arthroplast. 19 (2004) 84-87.

[20] H.G. Willert, G.H. Buchhorn, A. Fayyaz, R. Flury, M. Windler, G. Köster, C. H. Lohmann, J.Bone . Jt. Surg. 87 (2005) 28-36.

[21] M. Huber, G. Reinisch, G. Trettenhahn, K. Zweymuller, F. Lintner, Acta Biomater. 5 (2009) 172-180.

[22] R. Varano, J.D. Bobyn, J.B. Medley, S. Yue, Proc. Instn. Mech. Engrs. H 220 (2006) 145-159.

[23] A. Chiba, K. Kumagai, N. Nomura, S. Miyakawa, Acta Mater. 55 (2007) 1309-1318.

[24] A.J. Saldivar-Garcia, H.F. Lopez, J. Biomed. Mater. Res. A 74 (2005) 269-274 .

[25] A.J. Saldivar Garcia, A. Mani Medrano and A. Salinas Rodriguez, Scripta Mater. 40 (1999) 717-722.

[26] A.J. Saldivar Garcia, A. Mani Medrano and A. Salinas Rodriguez, Metall. Mater. Trans. 30A (1999) 1177-1184.

[27] M. Herrera, Espinoza, J. Mendez, M. Castro, J. Lopez, J. Rendon, J. Mater. Sci.: Mater. Med. 16 (2005) 607-611.

[28] M. Caudillo, M. Herrera-Trejo, M. R. Castro, E. Ramirez, C. R. Gonzalez, J.J. Juarez, J. Biomed. Mater. Res. 59 (2002) 378-385.

[29] J. Cawley, J.E.P. Metcalf, A.H. Jones, T.J. Band, D.S. Skupien, Wear 255 (2003) 999-1006.

[30] S. Spriano, E. Vernè, M.G. Faga, S. Bugliosi, G. Maina, Wear 259 (2005) 919-925.

[31] C. Balagna, S. Spriano, M.G. Faga, J. Nanosci. Nanotech. 11 (2011) 8994-9002.

[32] C. Balagna, M.G. Faga, S. Spriano, Mater. Sci. Eng. C 32 (2012) 887-895.

[33] S. Spriano, S. Bugliosi, WO 2006/038202A2 (2006).

[34] J. Black, Clin. Mater. 16 (1994) 167-173.

[35] B.R. Levine, S. Sporer, R.A. Poggie, C.J. Della Valle, J.J. Jacobs, Biomaterials 27 (2006) 4671-4681.

[36] D.M. Findlay, K. Welldon, G.J. Atkins, D.W. Howie, A.C.W. Zannettino, D. Bobyn, Biomaterials 25 (2004) 2215-2227.

[37] M. Stiehler, M. Lind, T. Mygind, A. Baatrup, A. Dolatshashi-Pirouz, H. Li, M. Foss, F. Besenbacher, M.Kassem, C. Bunger, J. Biomed. Mater. Res. A (2007) 448-458.

[38] S.M. Cardone, P. Kumar, C.A. Michaluk, H.D. Schwartz, Int. J. Refract. Met. Hard Mater. 13 (1995) 187-194.

[39] M.D. Bermudez, F. J. Carrion, G. Martınez-Nicolas, R. Lopez, Wear 258 (2005) 693–700.

[40] A. Robin, J. L. Rosa, Int. J. Refract. Met. Hard Mater. 18 (2000) 13-21.

[41] A.J. Saldivar-Garcia, H.F. Lopez, Scripta Mater. 45 (2001) 427-433.

[42] H.F. Lopez, A.J. Saldivar-Garcia, Metall. Mater. Trans. 39A (2008) 8-18.

[43] M. Sage, Ch. Guillaud, Rev. Met. 47 (1950) 139-145.

[44] D. Klarstrom, P. Crook, J. Wu, ASM Handbook 9, ASM International (2004) 762-774.

[45] ISO 3327:1982 (1982).

[46] ISO 7206-2:1996 (1996).

Figures

Fig.1. Comparison of the carbides distribution, size and dimensions before (on the left) and after (on the right) the thermal treatment: (a,b) HC-W, (c,d) HC-PM, (e,f) HC-C, (g, h) LC-C. EDS analysis referred to (i) Cr-carbide, (l) Mo-Carbide, (m) alloy area

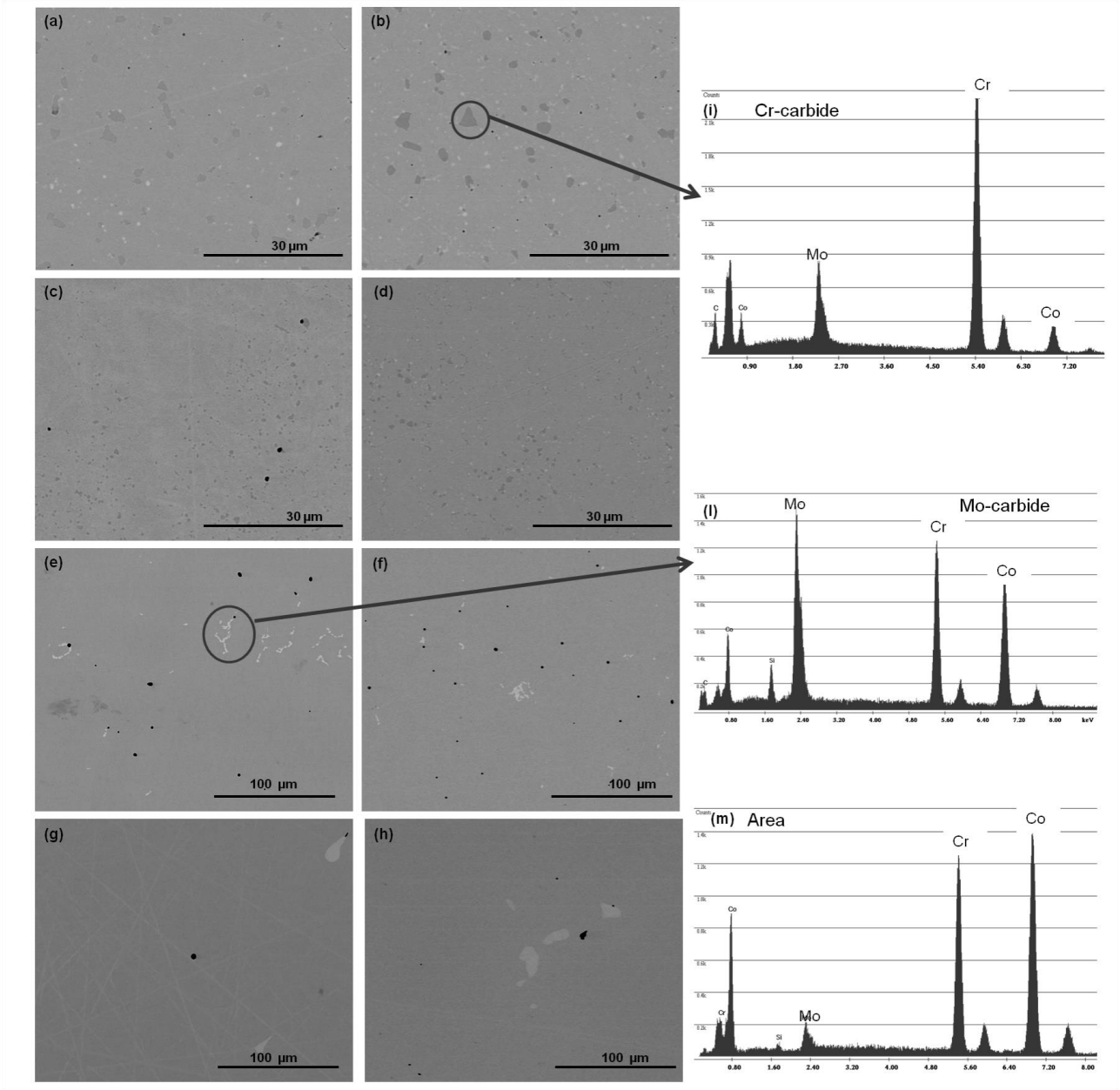

Fig.2. XRD analysis of high carbon alloys comparing the diffractograms before and after the thermal treatment, (a) HC-W and HC-W970sub, (b) HC-PM and HC-PM970sub, (c) HC-C and HC-C970sub

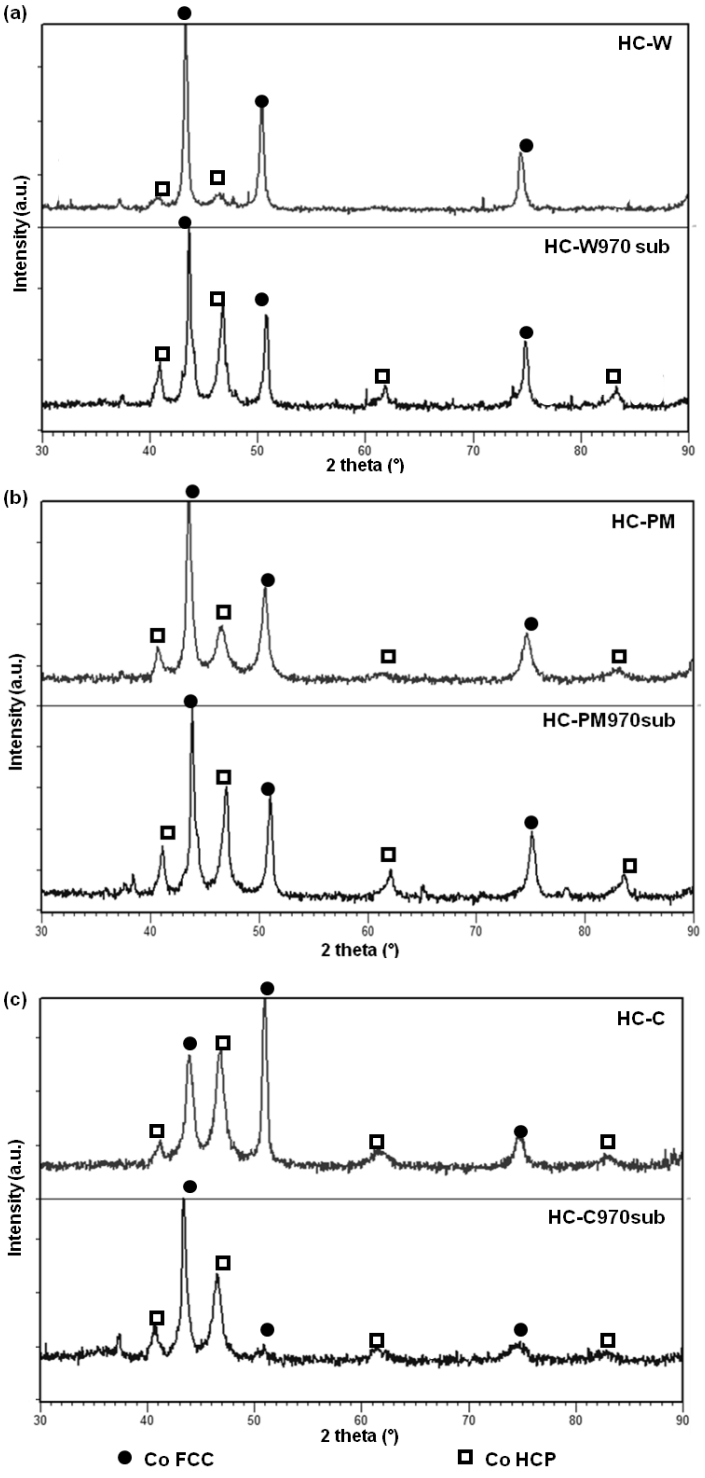

Fig.3. XRD analysis of low carbon alloys, comparing the diffractograms before and after the thermal treatment, (a) LC-W and LC-W970sub, (b) LC-C and LC-C970sub

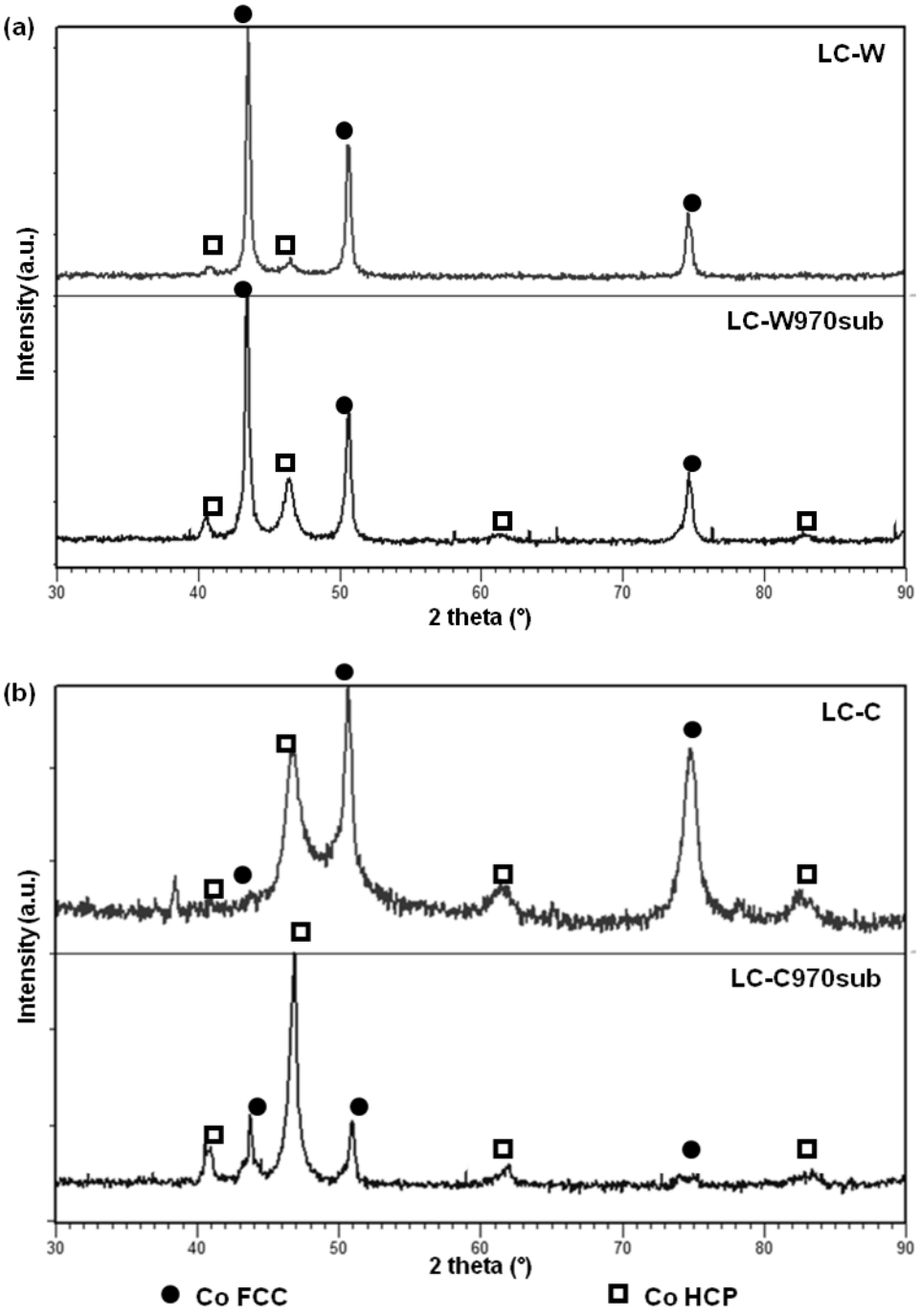

Fig.4. Photographs of the microstructure of the alloys, before (on the left) and after (on the right) thermal treatment: (a and b) HC-W, (c and d) HC-PM, (e and f) HC-C, (g and h) LC-C. Circle and arrows indicate carbides and grain boundaries

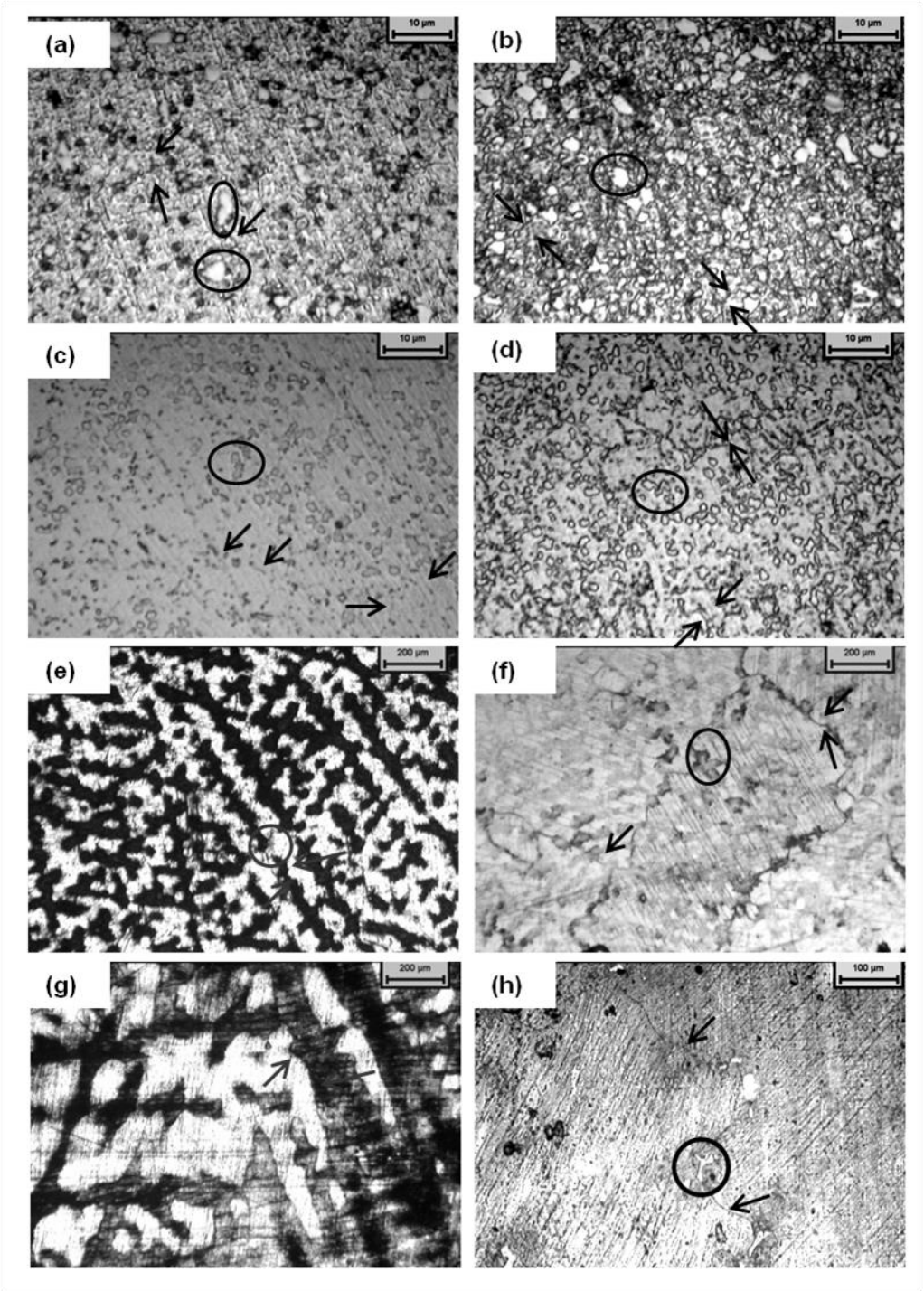

Fig.5. SEM micrographs ofdark HCP phase nucleated close to carbides (circles) or at grain boundaries (arrows) on (a) HC-C970sub and (b) LC-C970sub

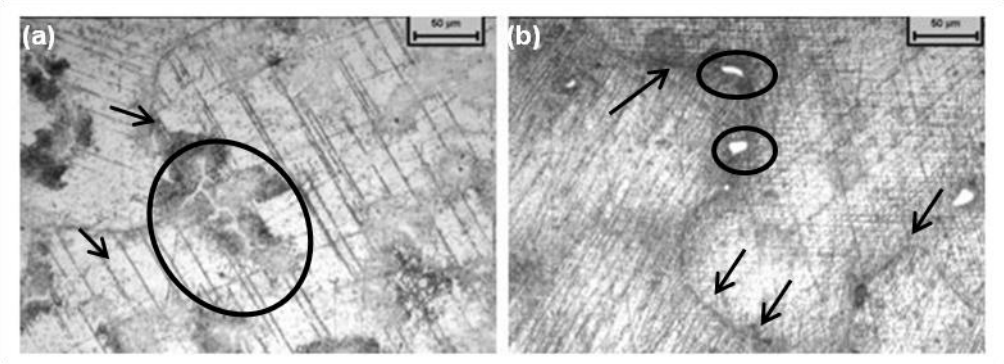

Fig.6. Load-displacement curves relative to the 3-point bending test

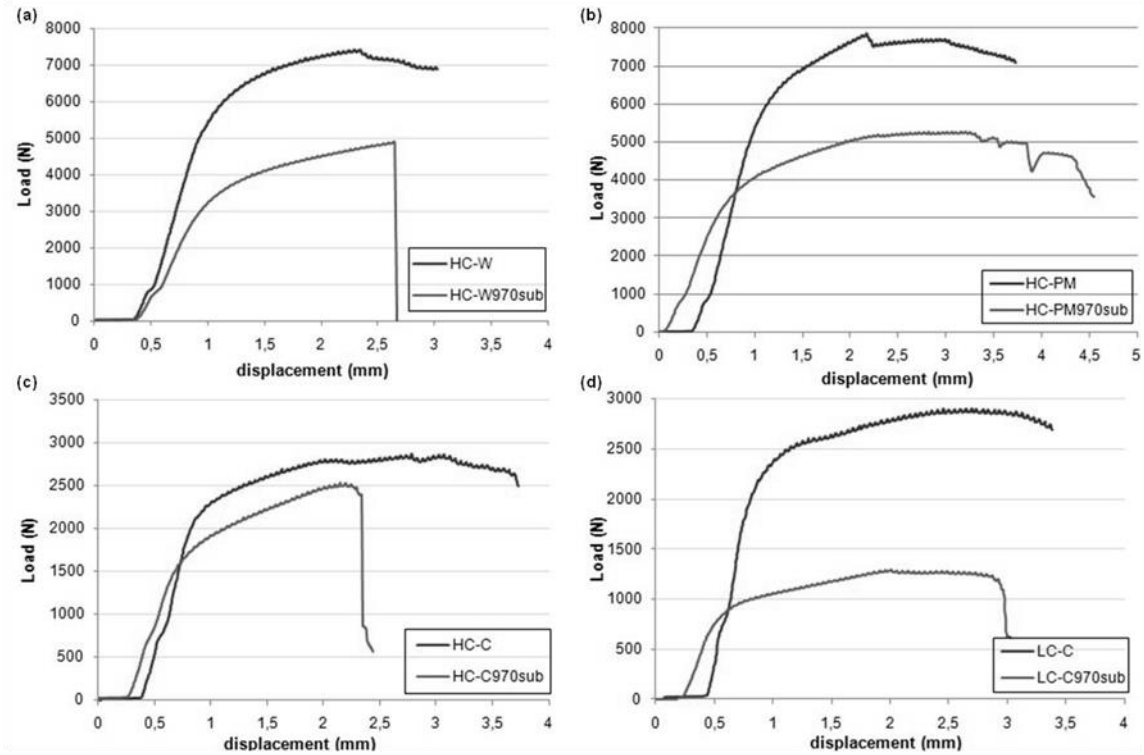

Fig.7. SEM images relative to surface fracture of HC-W970sub after bending test. The circles indicate fractured Cr-carbides

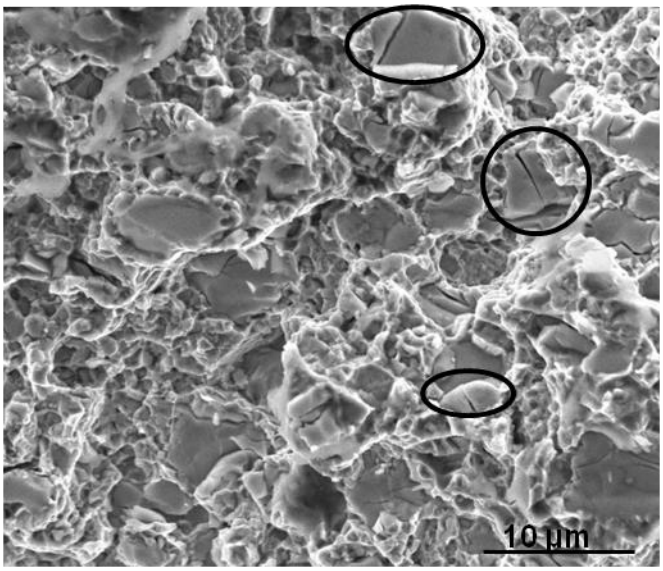

Fig.8. Wear track profiles of the as-received alloys and treated substrates after the ball on disc test : (a) HC-W, (b) HC-PM, (c) HC-C, (d) LC-C

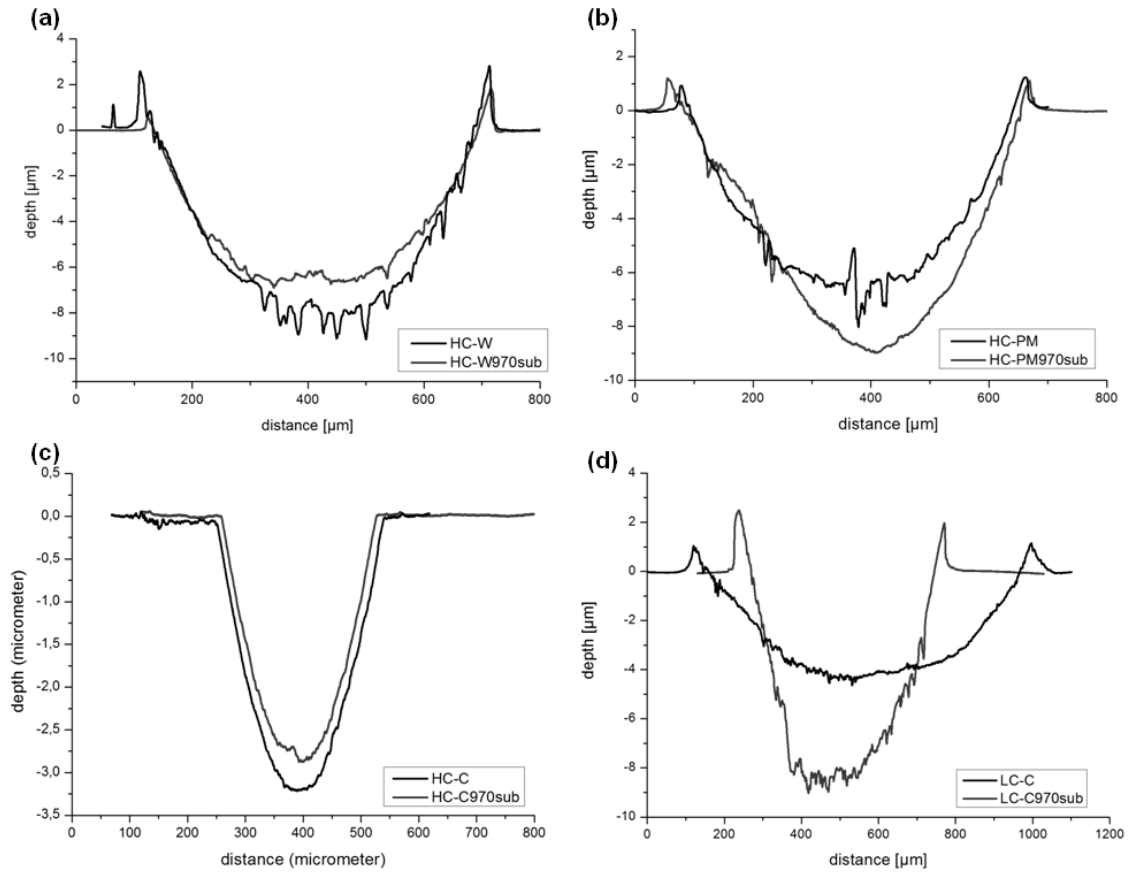

Fig.9. SEM micrographs at different magnifications relative to the wear track produced by an alumina ball on the HC-C surface evidencing molybdenum carbides (light circle) and the hole left by the pulling-out of the chromium carbides (dark circle)

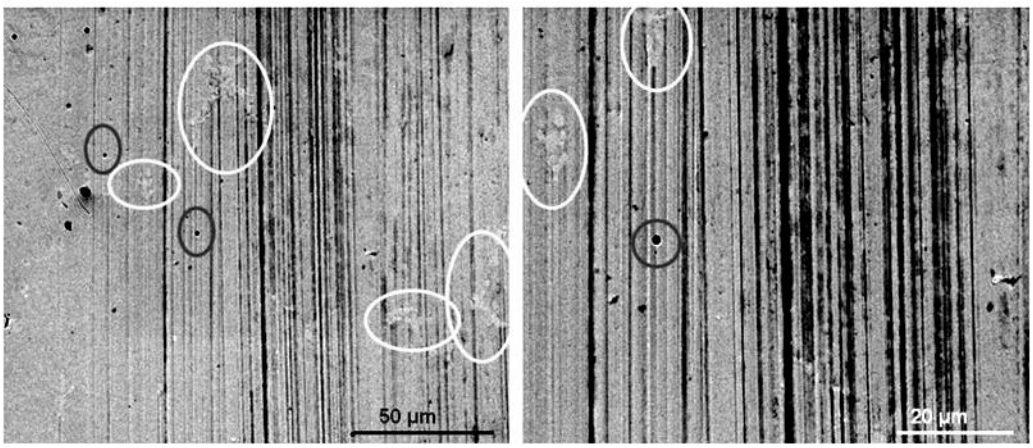

Tables

Table 1
Dimensions of samples analyzed at 3-points bending test

Sample	b (mm)	d (mm)
HC-W	6.5	3.5
HC-W970sub	6.5	3.0
HC-PM	6.5	3.5
HC-PM970sub	6.5	3.0
HC-C	6.5	3.3
HC-C970sub	6.5	2.8
LC-C	6.5	2.9
LC-C970sub	6.5	2.5

Table2
Composition of the as-received CoCrMo alloys

Alloy	Manufacturing process	EDS analysis				Quantometer analysis
		%wt. Co	%wt Cr	%wt Mo	%wt Ni	%wt C
HC-W	Wrought	62.5	30.6	6.4	0.5	0.25
HC-PM	Powder Metallurgy	66.2	28.1	6	-	0.14
HC-C	Casting	66.2	29.8	3.9	0.1	0.20
LC-W	Wrought	65.0	29.0	5.8	0.2	< 0.01
LC-C	Casting	64.1	33.5	2.4	-	0.07

Table 3
Roughness data relative to as received alloys and the substrates after the coating removal

Sample	Ra (nm)	Rq (nm)	Rz (nm)
HC-W	2±0.5	3±1	19±5
HC-W970sub	2±0.5	3±1	15±3
HC-PM	1±0.2	2±1	10±2
HC-PM970sub	3±0.3	4±1	19±4
HC-C	6±1	9±1	60±6
HC-C970sub	3±1	4±2	22 ±10
LC-W	6±1	6±1	28±2
LC-W970sub	4±0.4	5±1	26±4
LC-C	3±2	4±2	25±10
LC-C970sub	3±0.4	3±1	17±5

Table 4
The amount of the cubic and hexagonal phases in the as-received alloys and in the treated substrates, calculated in terms of percentage volume fraction with the three methods.

Sample	Volume fraction (%)					
	(1)		(2)		MAUD	
	FCC	HCP	FCC	HCP	FCC	HCP
HC-W	99	1	99	1	97 ± 4	3 ± 0.3
HC-W970sub	57	43	75	25	55 ± 1	45 ± 1
HC-PM	81	19	87	13	70 ± 2	30 ± 1
HC-PM970sub	58	42	75	25	58 ± 1	42 ± 1
HC-C	74	26	68	32	44 ± 2	55 ± 3
HC-C970sub	10	90	70	30	37 ± 6	63 ± 9
LC-W	98	2	99	1	-	-
LC-W970sub	85	15	87	13	54 ± 2	46 ± 2
LC-C	74	26	71	29	-	-
LC-C970sub	15	85	39	61	15 ± 2	85 ± 8

Table 5
Micro-hardness values evaluated under loads of 100g and 500g and macro-hardness values obtained under a load of 40kg.

Sample	HV 100g	HV 500g	HV 40 kg
HC-W	594 ± 23	588 ± 27	450 ± 13
HC-W970sub	509 ± 39	469 ± 3	441 ± 16
HC-PM	587 ± 13	574 ± 14	520 ± 12
HC-PM970sub	538 ± 27	492 ± 10	474 ± 13
HC-C	398 ± 26	382 ± 10	315 ± 15
HC-C970sub	396 ± 10	378 ± 20	347 ± 6
LC-W	509 ± 5	445 ± 8	-
LC-W970sub	439 ±10	499 ± 11	409 ± 18
LC-C	384 ± 5	320 ± 7	267 ± 25
LC-C970sub	429 ± 12	429 ± 38	287 ± 5

Table 6
Data obtained from the 3-point bending test

Sample	D (mm)	P (N)	σ (MPa)	ε	E (GPa)
HC-W	2.3	7412	2304	0.18	32.65
HC-W970sub	2.6	4919	2346	0.14	46.64
HC-PM	3.0	7692	2391	0.23	30.09
HC-PM970sub	2.3	5201	2480	0.12	46.14
HC-C	2.1	2814	984	0.15	18.73
HC-C970sub	2.2	2531	1386	0.11	34.14
LC-C	1.4	2624	828	0.18	10.76
LC-C970sub	2.0	1294	893	0.09	39.25